Experimental Quantum Channel Discrimination Using Metastable States of a Trapped Ion

Kyle DeBry,[1,2,*] Jasmine Sinanan-Singh,[1] Colin D. Bruzewicz,[2] David Reens,[2] May E. Kim,[2] Matthew P. Roychowdhury,[2] Robert McConnell,[2] Isaac L. Chuang,[1] and John Chiaverini[2,3]

[1]*Department of Physics, Center for Ultracold Atoms, and Research Laboratory of Electronics, Massachusetts Institute of Technology, Cambridge, Massachusetts 02139, USA*

[2]*Lincoln Laboratory, Massachusetts Institute of Technology, Lexington, Massachusetts 02421, USA*

[3]*Massachusetts Institute of Technology, Cambridge, Massachusetts 02139, USA*

(Received 2 June 2023; accepted 17 August 2023; published 25 October 2023)

We present experimental demonstrations of accurate and unambiguous single-shot discrimination between three quantum channels using a single trapped $^{40}Ca^{+}$ ion. The three channels cannot be distinguished unambiguously using repeated single channel queries, the natural classical analogue. We develop techniques for using the six-dimensional $D_{5/2}$ state space for quantum information processing, and we implement protocols to discriminate quantum channel analogues of phase shift keying and amplitude shift keying data encodings used in classical radio communication. The demonstrations achieve discrimination accuracy exceeding 99% in each case, limited entirely by known experimental imperfections.

DOI: 10.1103/PhysRevLett.131.170602

The indistinguishability of nonorthogonal states is one of the hallmarks of quantum mechanics, and it is both an obstacle and a resource. Much theoretical and experimental effort has been devoted to the task of quantum state discrimination [1–9] and its applications [10–12] over the past several decades. The related and far richer topic of quantum *channel* discrimination [13] is significantly more complex [14], and many channels can be distinguished unambiguously even when analogues states cannot [15,16]. These theoretical ideas open the door to exciting experimental probes of large classes of channels, including the widely used phase-shift keying (PSK) and amplitude-shift keying (ASK) channels, which classically encode data in phase or amplitude modulation of a carrier signal. These protocols have natural quantum analogues where the channels cannot be distinguished without error using semiclassical finite-length protocols [1,17].

Distinguishing among many quantum channels requires larger Hilbert spaces and more complex quantum gate sequences than binary channel discrimination, and these needs are well met by atomic systems. The long coherence times [18–20], high-fidelity single-qubit gates [19,21], and natural presence of many long-lived states [22] in atomic systems make them attractive for quantum protocols. More enticingly, atoms offer high-dimensional metastable state manifolds for encoding qudits or multiple qubits within a single atom [22–29], which are useful for discrimination among many channels. Additionally, atomic systems are well suited for electromagnetic sensing and communication, exemplified by the elegant use of Rydberg atoms for broadband signal detection and classical PSK and ASK protocols [30–33].

In this Letter, we experimentally demonstrate solutions to quantum channel discrimination problems constructed via the formalism of quantum signal processing (QSP) [34–36]. QSP enables the application of nearly arbitrary d-degree polynomial transformations of an operator acting on a quantum subsystem by interleaving the operator with $O(d)$ unitary processing rotations. Here, we extend the protocol developed in [16] to the larger Hilbert space of the $D_{5/2}$ and $S_{1/2}$ manifolds of a trapped $^{40}Ca^{+}$ ion and present experimental results for unambiguous channel discrimination among a triad of π rotations about nonorthogonal axes of the Bloch sphere (see Fig. 1); this quantum PSK scheme is a quantum channel analogue of the nonorthogonal Peres-Wootters states [37], imaginatively known as "Mercedes-Benz" states in classical signal processing [38]. Similarly, we demonstrate and compare this with a protocol for discriminating rotations of varying angles about a consistent axis to realize a quantum ASK scheme. In both cases, we achieve detection accuracy exceeding 99%, with the inaccuracy well explained by known experimental imperfections. We also describe how these protocols can be extended to distinguish n channels with $O(n)$ oracle queries.

Prior work.—Quantum channel discrimination for operators from a finite set is theoretically well understood [15,39–43], but there have been few experimental realizations. The experiments reported here realize and extend the results of [16], which give quantum algorithms with optimal query complexity that discriminate sets of quantum

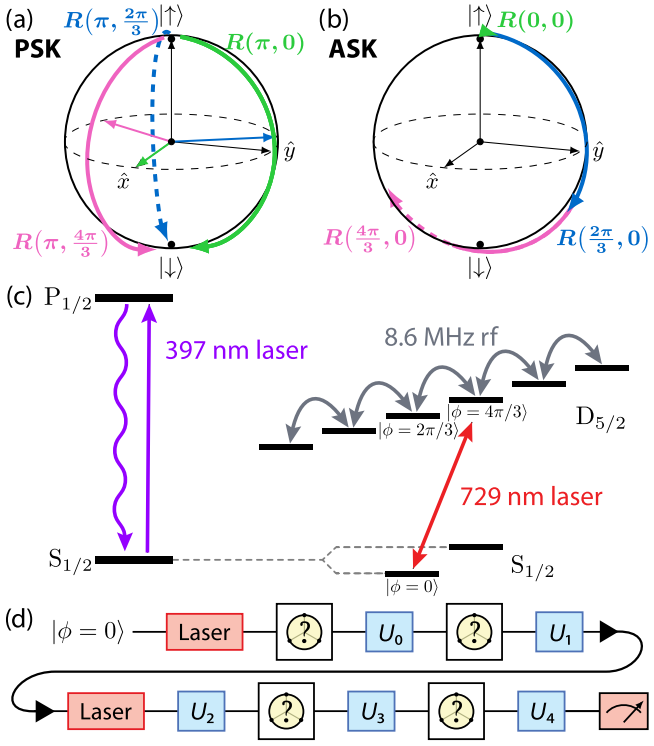

FIG. 1. Operations and atomic states used in the channel-discrimination protocols. (a) Bloch sphere showing PSK rotations, with colored arrows showing rotation axes at angles of 0, $2\pi/3$, and $4\pi/3$ in the $\hat{x}$–$\hat{y}$ plane, relative to $\hat{x}$. (b) Bloch sphere showing ASK rotations about $\hat{x}$. (c) Energy level diagram of the relevant states and transitions of $^{40}Ca^{+}$ ions. (d) Quantum circuit diagram for the PSK protocol. Gates shaded red are performed using the 729 nm laser, and all others are performed with the 8.6 MHz rf drive. Precomputed processing gates U_i are shaded blue. Gates labeled with the yellow question mark icon represent the oracle.

channels faithfully represented by a finite subgroup of SU(2). In this case, the unknown channel (the "oracle") is one of several possible unitary rotations. Single-shot oracle queries can distinguish such channels only with minimum error given by the Helstrom bound [17,44], which is $p_{\text{error}} = 1/3$ for the symmetric unitary channels investigated here [5,9,45]. Photonic systems have been used to discriminate between two such unitary channels using finite queries with [46] and without [47] entanglement. Discrimination between bosonic optical channels has also been realized in the framework of quantum reading [48]. Quantum process tomography has been realized in many physical systems, and such tomography can be used for channel discrimination, but aims at parameter measurement instead of making discrete decisions [14]. Recently, another application of quantum signal processing (for Hamiltonian simulation) was implemented on a trapped-ion system [49].

Methods.—We develop and implement pulse sequences to perform single-shot (requiring only a single trial) discrimination among three unitary channels using only four oracle queries per trial, based on the QSP-derived protocols in [16]. In particular, the three possible unitary rotations for our implementation of PSK are the π rotations of the Bloch sphere about different axes shown in Fig. 1(a): $R(\pi, 0)$, $R(\pi, 2\pi/3)$, or $R(\pi, 4\pi/3)$, where $R(\theta, \phi)$ represents a rotation of angle θ about the axis $(\hat{x}\cos\phi + \hat{y}\sin\phi)$. This version of the algorithm was developed using numerical optimization of pulse parameters. For the case of ASK channel discrimination, the oracle becomes one of the three rotations about the $\hat{x}$ axis shown in Fig. 1(b): $R(0, 0)$, $R(2\pi/3, 0)$, or $R(4\pi/3, 0)$. The ASK processing pulses were found by using PYQSP [36,50] to generate the quantum signal processing phases. In each case, the first half of the pulse sequence differentiates between signal angles (the oracle's angle ϕ or θ for PSK or ASK, respectively) 0 and $\neq 0$, and the second half differentiates signal angles $2\pi/3$ and $4\pi/3$. Each half is composed of the unknown signal operator interleaved between the precomputed processing gates. This is illustrated as a circuit diagram for the PSK case in Fig. 1(d). The pulse sequence for PSK (shown in a simplified form at the top of Fig. 2) is comprised of 24 laser and rf pulses, and the ASK sequence is comprised of 31 pulses. See the Supplemental Material [51] for the full pulse sequence parameters.

Although QSP is traditionally considered in the context of qubits (two-level systems), we have shown the ability to convert the qubit-based ASK algorithm given in [16] to both ASK and PSK algorithms in the six-level $D_{5/2}$ manifold of $^{40}Ca^{+}$ by proper consideration of the relevant SU(6) dynamics [58,59]. In particular, sequences of rotations that add up to the identity remain the identity, and sequences of rotations that add up to a bit flip operation in SU(2) likewise add up to the SU(6) generalization of a NOT gate. Figures 3(a) and 3(b) show how the response of the QSP algorithm (the population in each output state as a function of the oracle's signal angle θ or ϕ) changes when adapting the algorithm from SU(2) to SU(6). Specifically, the response of each algorithm is the same at the angles of interest (0, $2\pi/3$, and $4\pi/3$), but differs at other angles due to the differences in SU(2) and SU(6) dynamics. Figure 3(c) shows the response of the PSK protocol as a function of the phase ϕ in the $D_{5/2}$ manifold, where we observe twice as many peaks as in the ASK protocol [Fig. 3(b)]. This is because the algorithm transforms the PSK oracle with phase ϕ into an ASK oracle with angle $\theta = 2\phi$, leading to an ambiguity when distinguishing even numbers of channels. In the Supplemental Material [51], we describe in detail the relationship between SU(2) (qubit) and SU(6) ($D_{5/2}$ manifold) rotations, the transformation of ASK oracles into PSK oracles, and the resolution of this even-channel-number PSK ambiguity using a single extra oracle query.

Our experiment takes advantage of the extended Hilbert space of ground and metastable states in single $^{40}Ca^{+}$ ions.

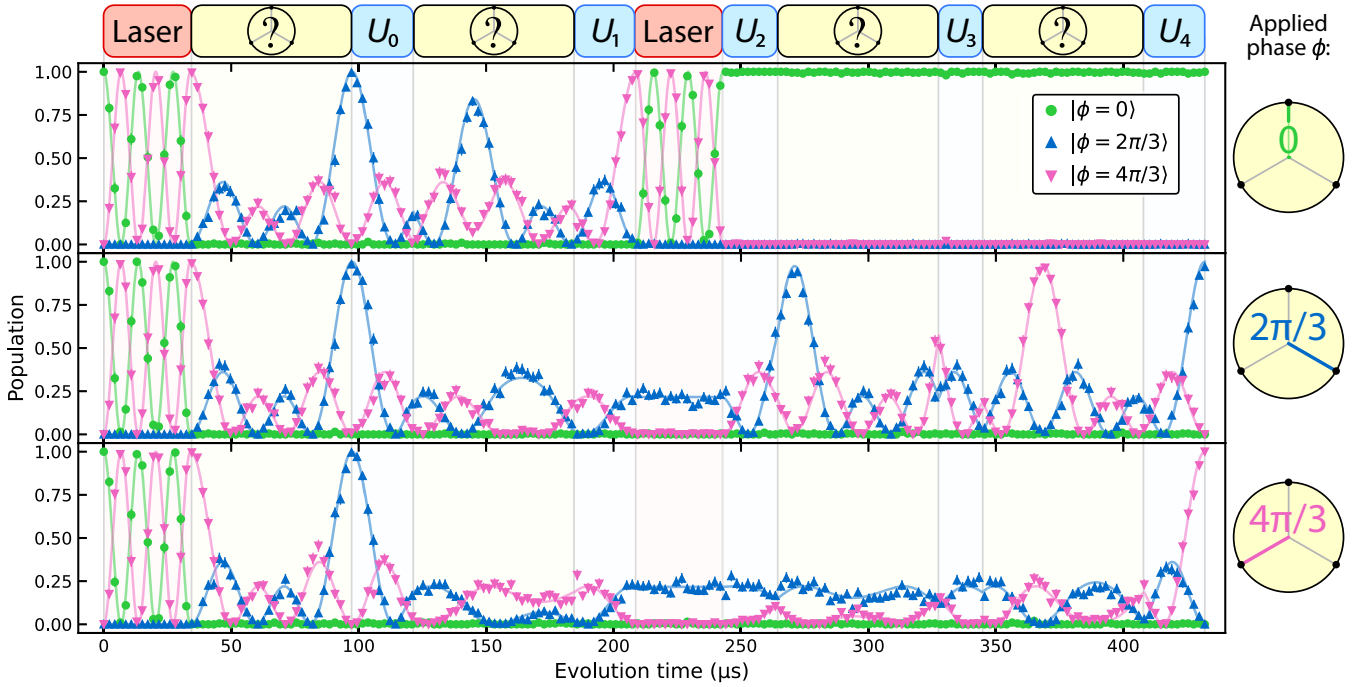

FIG. 2. Experimental data of the three-phase PSK algorithm as a function of evolution time. The pulse sequence representation along the top has colors and labels matching those in Fig. 1(d). The chart below is lightly shaded to highlight when each pulse is being applied. The phase of the oracle's π pulse is indicated on the right side of the figure. The three colors and shapes of points correspond to the probability of measuring each readout state [see Fig. 1(c)]. Each point corresponds to 200 trials, and the experimental data are overlaid on a zero-free-parameter simulation of the expected performance of the algorithm, displayed as solid lines. Error bars represent 1σ confidence intervals.

We make use of states from the $D_{5/2}$ manifold for processing and the $S_{1/2}$ manifold for shelving and readout. We label our three PSK algorithm readout states $|\phi = 0\rangle$ in the $S_{1/2}$ manifold, and $|\phi = 2\pi/3\rangle$ and $|\phi = 4\pi/3\rangle$ in the $D_{5/2}$ manifold, as depicted in Fig. 1(c). Ions are confined in a cryogenic surface-electrode trap at 5 K, similar to systems described previously [60,61]. The oracle is applied as an 8.6 MHz radio frequency (rf) signal from a small antenna located inside the coldest stage of the cryostat, approximately 3 cm from the ion. In the PSK case, the oracle rotations are realized by fixed-length pulses with phases of 0, $2\pi/3$, or $4\pi/3$, the same as classical ternary PSK. The rf antenna is also used to apply the processing gates, and all rf pulses act solely on the $D_{5/2}$ manifold. Additionally, a narrow linewidth 729 nm laser is used to move population between the $S_{1/2}$ manifold and the $D_{5/2}$ manifold.

Laser-based shelving to the $S_{1/2}$ manifold allows us to adapt the multiqubit QSP sequence into a single-shot, single-ion algorithm. If the first half of the QSP sequence determines that the oracle's angle was 0, the population will be in the $|\phi = 4\pi/3\rangle$ state, and the following laser π pulse moves population to the state $|\phi = 0\rangle$ in the $S_{1/2}$ manifold (similar to "hiding" and "unhiding" pulses in [62]). Otherwise, population is in the other states of the $D_{5/2}$ manifold after the first half of the algorithm, so the laser pulse has no effect. The protocol then proceeds to differentiate between the remaining two angles. This pulse sequence is shown schematically at the top of Fig. 2.

Through these QSP sequences of oracle queries interleaved with precomputed processing pulses, we deterministically transfer population to different states according to the oracle value. The populated state is then determined using the following qudit-style readout scheme [22,25,28]. We first apply 397 nm detection light resonant with the $S_{1/2} \leftrightarrow P_{1/2}$ cycling transition [Fig. 1(c)] and look for fluorescence, which indicates the ion was in the $|\phi = 0\rangle$ state. If no fluorescence is observed, a laser π pulse is used to transfer the population from the $|\phi = 2\pi/3\rangle$ state to the ground state, and the detection beam is again applied. If there is again no fluorescence, the $|\phi = 4\pi/3\rangle$ population is transferred down and the fluorescence measurement is repeated a third time. We measure the population in all three readout states to detect any leakage out of this three-state space.

Sources of error.—There are two primary sources of error for this experiment that arise from use of the larger Hilbert space of trapped ion systems: control instability and level instability. Control instability refers to amplitude or phase fluctuations of the applied pulses, and level instability refers to fluctuations in the energy of states. We minimize control instability errors by taking advantage of

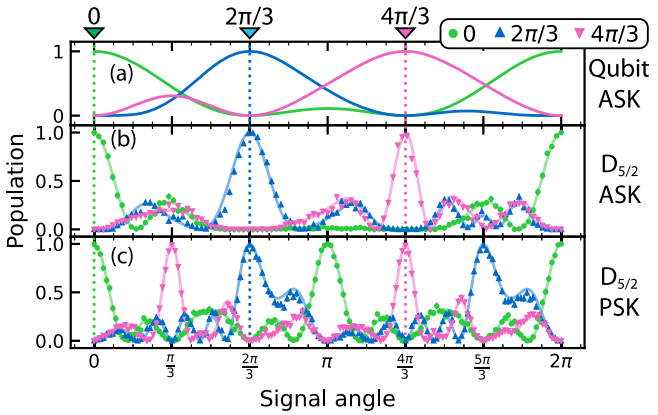

FIG. 3. Input-output plot showing the response of channel discrimination protocols as a function of the signal angle for the channel. For ASK protocols, the signal angle is the rotation angle θ, and for the PSK protocol it is the phase ϕ. Error bars represent 1σ confidence intervals, but are smaller than data point symbols in most cases. Data points correspond to 200 trials. (a) Theory curves for an ASK protocol implemented with qubits [SU(2)]. (b) ASK protocol performed in the $D_{5/2}$ manifold [SU(6)], with data points overlaid on solid theory curves. (c) PSK performed in the $D_{5/2}$ manifold [SU(6)], with data points overlaid on solid theory curves.

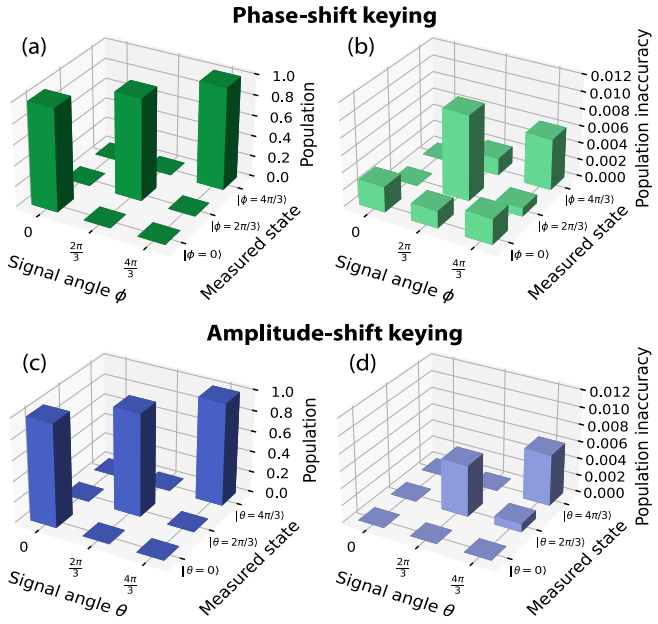

FIG. 4. Populations and magnitudes of population deviations from optimal (the 3×3 identity matrix) for each possible oracle value for both phase- and amplitude-shift keying implementations of the three-channel discrimination problem. The data for each signal angle correspond to 10 000 trials. (a) PSK populations. (b) Magnitude of PSK deviation from optimal. (c) ASK populations. (d) Magnitude of ASK deviation from optimal.

the superior phase and amplitude stability of the rf drive over laser pulses wherever possible by performing all the quantum information processing with the rf drive in the $D_{5/2}$ manifold. For the few remaining required laser π pulses, we use CP Robust 180 pulse sequences [63,64], which reduce laser-induced errors in our experiment by a factor of 5.

Use of the full manifold of states places strict requirements on the stability of the state's energy levels. The magnetic field sensitivity of Zeeman sublevels' energies passes this constraint on to the magnetic field, and we address this requirement both passively and actively. To achieve $> 99\%$ accuracy, the length of the algorithm and our experimental parameters dictate that the rf drive must remain within 30 Hz of resonance, corresponding to a magnetic field stability of better than 20 μG. The cryogenic apparatus allows us to stabilize the magnetic field with two rings of superconducting niobium [61,65,66], enabling metastable Zeeman qubit coherence times of $T_2^* \approx 90$ ms (see Supplemental Material [51]). This stability is sufficient for a single trial taking less than 1 ms, but slow frequency drifts require compensation on the timescale of seconds, which we implement as an active feed-forward protocol. This clock-protocol-like scheme is described in the Supplemental Material [51]. This protocol brings magnetic-field-induced errors well below 1%, allowing us to take full advantage of these magnetic field-sensitive states.

Results.—We achieve better than 99% accuracy for both the ASK and PSK quantum channel discrimination algorithms. For the PSK case, the applied operator was correctly determined in $99.4^{+0.1}_{-0.2}\%$ of trials, averaged over the three possible oracle values. For the ASK case, we measure the correct output state with $99.6^{+0.1}_{-0.1}\%$ accuracy, even when applying a total of 31 pulses (see Supplemental Material [51]). Uncertainties represent 1σ confidence intervals computed using the Wilson score interval method [67,68]. The probability of detecting the ion in each of the three output states is shown in Figs. 4(a) and 4(c), with the population deviations from the ideal case shown in Figs. 4(b) and 4(d), for the PSK and ASK cases, respectively. A plot of the populations of the three readout states as a function of evolution time during the algorithm is shown in Fig. 2 for the PSK algorithm, demonstrating close agreement of the data with the analytic predictions (solid lines). Both versions of the algorithm are shown as a function of signal angle (θ or ϕ) in Fig. 3, again showing close agreement with predicted performance.

The inaccuracy is well explained by known error sources, and is dominated by control errors rather than intrinsic errors. We measure the inaccuracy due to state preparation, detection, and laser π pulses to be 0.21(5)%, and calculate the magnetic field-induced errors to be 0.2%–0.4% for the different versions of the algorithm by estimating the average detuning from resonance. Errors from spontaneous emission from the $D_{5/2}$ states during the duration of the experiment are $< 0.1\%$. All three of these error mechanisms could result in population leakage out of the three-state readout space, but with the current readout method, spontaneous emission appears not as leakage but

as measurement of an incorrect readout state. This is discussed in the Supplemental Material [51].

Outlook and conclusion.—The results we report here set the stage for the exploration of large sets of quantum channels. As expected from theory [16], these results show a quantum advantage over semiclassical and naïve quantum protocols (see the Supplemental Material [51]). Scaling this algorithm to n channels with equally spaced angles is straightforward and asymptotically optimal in query complexity [16], scaling as $O(n)$. We have also shown how to discriminate channels in the desirable case of phase-shift keying with an even number of angles with a single additional oracle query [51].

In conclusion, we have demonstrated entanglement-free discrimination of more than two quantum channels with finitely many queries of the operator, using a framework that can be scaled to many channels. We have demonstrated this protocol with single-shot readout by using the combined state space of the $D_{5/2}$ and $S_{1/2}$ manifolds of a trapped ion, including the development of novel quantum information processing techniques in the six-level $D_{5/2}$ manifold that highlight the quantum information processing potential of metastable states [23]. Because of atomic systems' ability to receive electromagnetic signals across an exceptionally broad frequency band, this opens the door to single-atom reception, decoding, and quantum processing of a wide range of classical and quantum signals.

We thank Z. M. Rossi and J. M. Martyn for helpful discussions. This research was supported by the U.S. Army Research Office through Grant No. W911NF-20-1-0037. This material is based upon work supported by the National Science Foundation Graduate Research Fellowship under Grant No. 2141064. K. D. acknowledges support from the MIT Center for Quantum Engineering–Laboratory for Physical Sciences Doc Bedard Fellowship. I. L. C. acknowledges support by the NSF Center for Ultracold Atoms. The opinions, interpretations, conclusions, and recommendations are those of the authors and are not necessarily endorsed by the U.S. Government.

*debry@mit.edu

[1] C. Helstrom, *Quantum Detection and Estimation Theory* (Academic Press, Inc., New York, 1976).
[2] R. L. Cook, P. J. Martin, and J. M. Geremia, Nature (London) **446**, 774 (2007).
[3] A. Chefles, Contemp. Phys. **41**, 401 (2000).
[4] S. M. Barnett and E. Riis, J. Mod. Opt. **44**, 1061 (1997).
[5] M. Ban, K. Kurokawa, R. Momose, and O. Hirota, Int. J. Theor. Phys. **36**, 1269 (1997).
[6] R. B. M. Clarke, V. M. Kendon, A. Chefles, S. M. Barnett, E. Riis, and M. Sasaki, Phys. Rev. A **64**, 012303 (2001).
[7] R. B. M. Clarke, A. Chefles, S. M. Barnett, and E. Riis, Phys. Rev. A **63**, 040305(R) (2001).
[8] G. Waldherr, A. C. Dada, P. Neumann, F. Jelezko, E. Andersson, and J. Wrachtrup, Phys. Rev. Lett. **109**, 180501 (2012).
[9] M. A. Solís-Prosser, M. F. Fernandes, O. Jiménez, A. Delgado, and L. Neves, Phys. Rev. Lett. **118**, 100501 (2017).
[10] N. Gisin, G. Ribordy, W. Tittel, and H. Zbinden, Rev. Mod. Phys. **74**, 145 (2002).
[11] G. Chesi, S. Olivares, and M. G. A. Paris, Phys. Rev. A **97**, 032315 (2018).
[12] S. Pirandola, U. L. Andersen, L. Banchi, M. Berta, D. Bunandar, R. Colbeck, D. Englund, T. Gehring, C. Lupo, C. Ottaviani *et al.*, Adv. Opt. Photonics **12**, 1012 (2020).
[13] S. Pirandola, R. Laurenza, C. Lupo, and J. L. Pereira, npj Quantum Inf. **5**, 1 (2019).
[14] M. A. Nielsen and I. L. Chuang, *Quantum Computation and Quantum Information* (Cambridge University Press, Cambridge, England, 2000).
[15] Q. Zhuang and S. Pirandola, Phys. Rev. Lett. **125**, 080505 (2020).
[16] Z. M. Rossi and I. L. Chuang, Phys. Rev. A **104**, 012425 (2021).
[17] U. Herzog and J. A. Bergou, Phys. Rev. A **65**, 050305(R) (2002).
[18] T. Ruster, C. T. Schmiegelow, H. Kaufmann, C. Warschburger, F. Schmidt-Kaler, and U. G. Poschinger, Appl. Phys. B **122**, 254 (2016).
[19] T. P. Harty, D. T. C. Allcock, C. J. Ballance, L. Guidoni, H. A. Janacek, N. M. Linke, D. N. Stacey, and D. M. Lucas, Phys. Rev. Lett. **113**, 220501 (2014).
[20] P. Wang, C.-Y. Luan, M. Qiao, M. Um, J. Zhang, Y. Wang, X. Yuan, M. Gu, J. Zhang, and K. Kim, Nat. Commun. **12**, 233 (2021).
[21] C. Sheng, X. He, P. Xu, R. Guo, K. Wang, Z. Xiong, M. Liu, J. Wang, and M. Zhan, Phys. Rev. Lett. **121**, 240501 (2018).
[22] P. J. Low, B. M. White, A. A. Cox, M. L. Day, and C. Senko, Phys. Rev. Res. **2**, 033128 (2020).
[23] D. Allcock, W. Campbell, J. Chiaverini, I. Chuang, E. Hudson, I. Moore, A. Ransford, C. Roman, J. Sage, and D. Wineland, Appl. Phys. Lett. **119**, 214002 (2021).
[24] H.-X. Yang, J.-Y. Ma, Y.-K. Wu, Y. Wang, M.-M. Cao, W.-X. Guo, Y.-Y. Huang, L. Feng, Z.-C. Zhou, and L.-M. Duan, Nat. Phys. **18**, 1058 (2022).
[25] M. Ringbauer, M. Meth, L. Postler, R. Stricker, R. Blatt, P. Schindler, and T. Monz, Nat. Phys. **18**, 1053 (2022).
[26] P. Hrmo, B. Wilhelm, L. Gerster, M. W. van Mourik, M. Huber, R. Blatt, P. Schindler, T. Monz, and M. Ringbauer, Nat. Commun. **14**, 2242 (2023).
[27] K. Sun, C. Fang, M. Kang, Z. Zhang, P. Zhang, D. N. Beratan, K. R. Brown, and J. Kim, arXiv:2304.12247.
[28] W. C. Campbell and E. R. Hudson, arXiv:2210.15484.
[29] D. González-Cuadra, T. V. Zache, J. Carrasco, B. Kraus, and P. Zoller, Phys. Rev. Lett. **129**, 160501 (2022).
[30] D. H. Meyer, K. C. Cox, F. K. Fatemi, and P. D. Kunz, Appl. Phys. Lett. **112**, 211108 (2018).
[31] M. T. Simons, A. H. Haddab, J. A. Gordon, and C. L. Holloway, Appl. Phys. Lett. **114**, 114101 (2019).
[32] D. H. Meyer, Z. A. Castillo, K. C. Cox, and P. D. Kunz, J. Phys. B **53**, 034001 (2020).

[33] C. T. Fancher, D. R. Scherer, M. C. S. John, and B. L. S. Marlow, IEEE Trans. Quantum Eng. **2**, 1 (2021).
[34] G. H. Low and I. L. Chuang, Phys. Rev. Lett. **118**, 010501 (2017).
[35] G. H. Low and I. L. Chuang, Quantum **3**, 163 (2019).
[36] J. M. Martyn, Z. M. Rossi, A. K. Tan, and I. L. Chuang, PRX Quantum **2**, 040203 (2021).
[37] A. Peres and W. K. Wootters, Phys. Rev. Lett. **66**, 1119 (1991).
[38] J. Kovačević and A. Chebira, Found. Trends Signal Process. **2**, 1 (2008).
[39] A. Acín, Phys. Rev. Lett. **87**, 177901 (2001).
[40] G. M. D'Ariano, P. LoPresti, and M. G. A. Paris, Phys. Rev. Lett. **87**, 270404 (2001).
[41] R. Duan, Y. Feng, and M. Ying, Phys. Rev. Lett. **98**, 100503 (2007).
[42] R. Duan, Y. Feng, and M. Ying, Phys. Rev. Lett. **103**, 210501 (2009).
[43] K. Nakahira and K. Kato, Phys. Rev. A **103**, 062606 (2021).
[44] A. Chefles, Phys. Lett. A **239**, 339 (1998).
[45] J. Bae and L.-C. Kwek, J. Phys. A **48**, 083001 (2015).
[46] A. Laing, T. Rudolph, and J. L. O'Brien, Phys. Rev. Lett. **102**, 160502 (2009).
[47] P. Zhang, L. Peng, Z.-W. Wang, X.-F. Ren, B.-H. Liu, Y.-F. Huang, and G.-C. Guo, J. Phys. B **41**, 195501 (2008).
[48] G. Ortolano, E. Losero, S. Pirandola, M. Genovese, and I. Ruo-Berchera, Sci. Adv. **7**, eabc7796 (2021).
[49] Y. Kikuchi, C. M. Keever, L. Coopmans, M. Lubasch, and M. Benedetti, arXiv:2303.05533.
[50] R. Chao, D. Ding, A. Gilyen, C. Huang, and M. Szegedy, arXiv:2003.02831.
[51] See Supplemental Material at http://link.aps.org/supplemental/10.1103/PhysRevLett.131.170602 for additional experimental and theoretical considerations, which includes [52–57].
[52] C. D. Bruzewicz, R. McConnell, J. Chiaverini, and J. M. Sage, Nat. Commun. **7**, 13005 (2016).
[53] C. Roos, T. Zeiger, H. Rohde, H. C. Nägerl, J. Eschner, D. Leibfried, F. Schmidt-Kaler, and R. Blatt, Phys. Rev. Lett. **83**, 4713 (1999).
[54] J. A. Sherman, M. J. Curtis, D. J. Szwer, D. T. C. Allcock, G. Imreh, D. M. Lucas, and A. M. Steane, Phys. Rev. Lett. **111**, 180501 (2013).
[55] O. Băzăvan, S. Saner, M. Minder, A. C. Hughes, R. T. Sutherland, D. M. Lucas, R. Srinivas, and C. J. Ballance, Phys. Rev. A **107**, 022617 (2023).
[56] J. A. Bergou, U. Futschik, and E. Feldman, Phys. Rev. Lett. **108**, 250502 (2012).
[57] P. Giorda, P. Zanardi, and S. Lloyd, Phys. Rev. A **68**, 062320 (2003).
[58] R. J. Cook and B. W. Shore, Phys. Rev. A **20**, 539 (1979).
[59] M. J. Curtis, Measurement-selected ensembles in trapped-ion qubits, Ph.D. thesis, Oxford University, 2010.
[60] J. M. Sage, A. J. Kerman, and J. Chiaverini, Phys. Rev. A **86**, 013417 (2012).
[61] C. Bruzewicz, R. McConnell, J. Stuart, J. Sage, and J. Chiaverini, npj Quantum Inf. **5**, 102 (2019).
[62] J. T. Barreiro, P. Schindler, O. Gühne, T. Monz, M. Chwalla, C. F. Roos, M. Hennrich, and R. Blatt, Nat. Phys. **6**, 943 (2010).
[63] C. A. Ryan, J. S. Hodges, and D. G. Cory, Phys. Rev. Lett. **105**, 200402 (2010).
[64] J. E. Christensen, D. Hucul, W. C. Campbell, and E. R. Hudson, npj Quantum Inf. **6**, 35 (2020).
[65] G. Gabrielse, J. Tan, P. Clateman, L. Orozco, S. Rolston, C. Tseng, and R. Tjoelker, J. Magn. Reson. **91**, 564 (1991).
[66] S. X. Wang, J. Labaziewicz, Y. Ge, R. Shewmon, and I. L. Chuang, Phys. Rev. A **81**, 062332 (2010).
[67] E. B. Wilson, J. Am. Stat. Assoc. **22**, 209 (1927).
[68] The Wilson score interval is recommended by statisticians over the commonly used Wald interval; L. D. Brown, T. T. Cai, and A. DasGupta, Stat. Sci. **16**, 101 (2001).